Quantifying the helium and hydrocarbon accumulation processes using noble gases in the North Qaidam Basin, China

Wen Zhang [a, b, c], Yuhong Li [a,*], Fenghua Zhao [d], Wei Han [a], Junlin Zhou [a], Greg Holland [e], Zheng Zhou [b, **]

a. Xi'an Center, China Geological Survey, 710054, China

b. Lancaster Environment Centre, Lancaster University, LA1 4YQ, UK

c. Institute of Geology, Chinese Academy of Geological Sciences, Beijing 100037, China

d. College of Geoscience and Surveying Engineering, China University of Mining and Technology, 100083, Beijing, China

e. School of Earth and Environmental Sciences, The University of Manchester, M13 9PL, UK

Abstract: Limited reserves and insecure resource supply have led to global shortage crises in helium, a vital gas for cryogenic engineering and other countless industrial manufacturing processes. Despite the attention drawn by global supply disruptions, the helium accumulation mechanism in natural gas fields remains poorly understood. Noble gases are excellent tracers for studying migration and accumulation processes of fluids in the subsurface and can be used to investigate the influence of subsurface fluids on helium accumulation. We present noble gas isotope and abundance data as well as major gas compositional data from 10 producing wells in three gas fields in the North Qaidam Basin, China. Helium is more concentrated in the Mabei and Dongping gas fields (2.06 - 48.4 $\times 10^{-4}$ cm^3 STP/cm^3) than in the Niudong gas field (1.15 - 1.42$\times 10^{-}$

* Correspondence to: No. 438, Youyi East Road, Beilin District, Xian, China.
** Corresponding author.
E-mail address: wenzhangcn@outlook.com (Wen Zhang); lyuhong@mail.cgs.gov.cn (Yuhong Li); z.zhou4@lancaster.ac.uk (Zheng Zhou);

^{4} cm^{3} STP/cm^{3}). The helium is mainly radiogenic, with $^{3}He/^{4}He$ ratios of 0.01-0.05 Ra, where Ra is the atmospheric value of $^{3}He/^{4}He$, and lacks significant contribution from the mantle (0.03-0.67%). The noble gases derived from air-saturated water (^{20}Ne, ^{36}Ar, ^{84}Kr and ^{130}Xe) can be explained by an oil-modified groundwater-exsolution model with excess heavy noble gases. The calculated V_{oil}/V_{water} and V_{gas}/V_{water} ratios indicate that the Mabei region is the most oil-rich area and the Dongping region has the driest natural gas, which is consistent with the geological context. These ratios further support the fractionation models. The strong linear relationship between ^{4}He and ^{20}Ne (R^{2}=0.98) suggested that ^{4}He was dissolved into groundwater before migrating into the oil or gas phase. The initial ^{4}He concentrations in groundwater can accumulate within 0.31-2.78 Myr assuming a ^{4}He flux from the entire crustal section. According to the fractionation model, helium in groundwater partitions into the gas phase when contacting hydrocarbons. The different volume ratios among oil, gas and water during the equilibration process cause much greater variability in the helium concentrations in the gas phase (e.g., 6.08×10^{-4} to 2.01×10^{-3} cm^{3} STP/cm^{3} in Mabei) than those in the groundwater phase (e.g. 9.18×10^{-3} to 1.39×10^{-2} cm^{3} ^{4}He STP/cm^{3} H_2O in Mabei). Hydrocarbons play a critical role in helium accumulation and dilution. Helium-rich natural gas fields are characterized by old groundwater systems and moderate hydrocarbon abundance. This study has succeeded in quantitatively assessing the helium accumulation process in natural gas fields in the North Qaidam Basin and revealed that both groundwater and hydrocarbon phases control the helium accumulation in the subsurface environment. This outcome has broad implications for the prediction of hydrocarbon and helium as resources.

Keywords: Noble gases; Hydrocarbon charge: Helium accumulation; North Qaidam Basin

1. Introduction

Helium is an important by-product of natural gas processing and liquefied natural gas (LNG) production. It is widely used in cryogenic engineering equipment, particularly the nuclear magnetic resonance imaging in medical diagnostics. It also has huge applications in space programmes, electronics, optical fibre manufacturing and scientific research (Cai et al., 2010; Nuttall et al., 2012, Boreham et al., 2018). The world has experienced shortages of helium twice, in 2006-2007 and 2013 (Ballentine, 2017; Bare et al., 2016). The imminent depletion of Bureau of Land Management (BLM) helium reserves in the U.S.A. and any future unstable helium supply from LNG production in Qatar are very likely to cause another "helium crisis". Therefore, it is urgent to better understand the helium accumulation mechanisms in natural gas fields.

^{4}He is produced by the radiogenic decay of ^{235}U, ^{238}U and ^{232}Th in minerals (Ballentine and Burnard, 2002). The release and diffusion of helium have been studied in many U- and Th-rich minerals, such as apatite, zircon, monazite, and titanite, and it has been demonstrated that, at temperatures below the closure temperature of the host mineral, helium is released from these minerals over geological timescales (Cherniak and Pyle, 2008; Cherniak and Watson, 2011; Farley, 2000; Reiners et al., 2002). After release, helium is transported into subsurface fluid system, where it is influenced by different fluids, such as oil, gas and groundwater. Previous studies suggested that there was a relationship between ^{4}He accumulation and groundwater movement (Ballentine and Lollar, 2002; Brown, 2010; Tolstikhin et al., 2017). However, despite their importance, the influences of hydrocarbons and groundwater on helium accumulation remain poorly constrained.

Noble gases are excellent tracers for a variety of subsurface fluid processes in hydrothermal, volcanic and petroleum systems (Ballentine et al., 2002; Barry et al., 2018; Cao et al., 2018; Darrah et al., 2015; Gilfillan et al., 2008; Holland et al., 2013). Due to their inert natures, noble gases are

rarely influenced by chemical reactions and biological processes (Ozima and Podosek, 2002). Noble gases in subsurface fluid systems can be classified as atmospheric, mantle or radiogenic components, each of which has distinct isotopic signatures (Ballentine et al., 2002). Air-derived noble gases (ADGs, e.g., ^{20}Ne and ^{36}Ar) dissolved into groundwater in the recharge area, are transported to the subsurface and are fractionated by the solubility differences in different phases. This fractionation allows an investigation into the nature of the different phases, the relative volumes involved and the migration processes that occur in the subsurface (Ballentine et al., 1991; Barry et al., 2016; Zartman et al., 1961; Zhou et al., 2005). In addition, ADGs have been applied in groundwater protection studies to identify the source of fugitive gas contamination in an aquifer (Darrah et al., 2014; Wen et al., 2017) and to estimate the influence of enhanced oil recovery on water resources (Barry et al., 2018). Radiogenic noble gases (e.g., ^{4}He, $^{21}Ne^{*}$, and $^{40}Ar^{*}$) have also been used to constrain the residence time of gas reservoirs and groundwaters in the subsurface (Holland et al., 2013; Pinti et al., 2011; Zhou and Ballentine, 2006; Zwahlen et al., 2017).

Since noble gases are a powerful tool to trace groundwater movement and hydrocarbon charging in the subsurface, which have major impacts on helium accumulation, the noble gas data from natural gas fields in the North Qaidam Basin can provide an excellent opportunity to address a number of key issues regarding helium and hydrocarbon accumulation processes in gas fields, such as the presence of oil and gas phases, the extent of phase equilibrium in open or closed systems, the volume ratios of different phases involved in the system (oil, gas and water), and the quantification of the influence of groundwater and hydrocarbons on helium enrichment and dilution.

2. Geological background

The Qaidam Basin, which has an area of approximately 121,000 km^2, is located in the northern part of the Qinghai-Tibet Plateau in China. Several gas and oil fields (e.g., Dongping, Niudong, Lenghu, Pingtai, Mabei, Nanbaxian, and Yuka) have been discovered in the North Qaidam Basin in the last 60 years (Fig. 1a). The predominant hydrocarbon source rocks in this area are Lower-Middle Jurassic strata, which are mainly classified as Type II-III and are composed of dark or grey-black mudstones, carbonaceous mudstones and coal (Li et al., 2016; Ma et al., 2015; Tian et al., 2017). Unlike the Niudong field, no hydrocarbon source rocks are present beneath the Mabei and Dongping gas fields (Fig. 1b), suggesting that the natural gas in the Mabei and Dongping fields migrated from adjacent depressions. The carbon isotope values of methane suggest that the maturity of the hydrocarbon source rocks in the North Qaidam Basin varies with vitrinite reflectance (Ro), which ranges from 0.85% to 4.76% (Tian et al., 2017). The gas reservoirs are mainly in the Xiaganchaigou Formation (E_3) in Mabei and in Jurassic strata (J_1) and the Ganchaigou Formation (E_3) in Niudong. Furthermore, the majority of the gas in Dongping is distributed in bedrock, which mainly consists of Neoproterozoic and early Palaeozoic granite and metamorphic rocks (Ma et al., 2015). Oil was mainly generated in the Miocene period (N_1), and gas was mainly generated after the Pliocene (N_2) (Luo et al., 2013).

3. Methodology

3.1 Sample collection

Gas samples (n=10) were collected in high-pressure stainless-steel cylinders from producing wellheads in three gas fields in the North Qaidam Basin: the Dongping gas field (n=3), the Mabei gas field (n=4), and the Niudong gas field (n=3). The high-pressure cylinders were flushed with

the produced gas for at least 5 min to evacuate air in the connecting pipes and all dead space prior to sample collection. Once samples were shipped to the laboratory in Xi'an Center, China Geological Survey, gas samples were decanted from the cylinders and transferred to refrigeration-grade copper tubes with an external diameter of 10 mm. A two-stage pressure regulator was used to step down the pressure from the well stream to 1-2 bars as the gas flowed into the copper tubes. The copper tubes were flushed with the produced gas for 10 min before being sealed with stainless-steel clamps (Zhang et al., 2019). The remaining gas in the cylinders was shipped to the Key Laboratory of Petroleum Resource Research, Chinese Academy of Sciences, Lanzhou, for major gas composition analysis and a complete suite of hydrocarbon gas composition tests. A MAT271 mass spectrometer (MS) and an on-line continuous flow gas chromatograph (GC) were used for these compositional analyses, as described in detail in Zhang et al. (2018). The analysis errors were less than 1 vol% for CH_4, CO_2 and N_2 and less than 10 vol% for other gases. The major gas component results of two samples (Mabei 1 and Dongping 3) were not acquired due to shipping loss.

3.2 Analytical techniques

Noble gas analyses were conducted in the subsurface fluid isotope geochemistry laboratory at the Lancaster Environment Centre, Lancaster University. Before gas was released from the copper tube to the high-vacuum prep line, a quadrupole MS (Hiden Analytical HAL-201) was used to detect any possible leak and eliminate air contamination during testing. First, samples were expanded into a calibrated volume, the pressure of which was detected using an MSK manometer. Then, the samples were expanded into the rest prep line for the purification and separation processes. Specifically, samples were expanded onto a Ti-sponge getter held at 800ºC and then cooled to room temperature for 20 mins to remove reactive gases and hydrocarbons, followed by

further cleaning using a hot getter (SAEC GP50) held at 250ºC for 15 mins. Noble gases were separated by a charcoal cold finger refrigerated by liquid nitrogen (trapping Ar, Kr and Xe) and a Janis cryogenic trap (trapping He and Ne).

All noble gases (He, Ne, Ar, Kr and Xe) were sequentially released from the cold finger and cryogenic trap. Two cold getters held at room temperature (SAES GP50) were used to further remove hydrogen prior to expanding the gas into the NGX noble gas mass spectrometer (IsotopX). Due to the overlap of release temperature, Ar and Kr were released simultaneously but measured separately by releasing the gas stored in different segregated lines into the NGX. The concentration and all isotopic ratios of the five noble gases were determined. Doubly charged $^{40}Ar^{++}$ and CO_2^{++} were measured to correct ^{20}Ne and ^{22}Ne following the methods of Niedermann et al. (1993).

Blanks were measured once per week following the same procedures as used for the samples. The average blank corrections for ^{4}He, ^{20}Ne, ^{40}Ar, ^{84}Kr and ^{130}Xe were 0.29 vol.%, 0.05 vol.%, 1.28 vol.%, 0.06 vol.% and 0.57 vol.%, respectively. An air standard was analyzed each day to ensure the stability and reproducibility of the system.

4. Results

4.1 Major gas compositions

Major gas compositions from 8 wells are shown in Table 1. The produced gases primarily consist of methane (C_1), ranging from 76.64 vol% to 95.18 vol%, with minor longer-chain hydrocarbons (C_2 and C_3). Gas dryness (C_1/C_{1-5}) (Lorant et al., 1998) is an indicator of hydrocarbon maturity because longer-chain hydrocarbons tend to crack into short-chain molecules at a higher temperature or over longer time periods (Behar et al., 1997). Gas dryness was calculated to be 0.97 in Dongping, 0.89-0.91 in Niudong, and 0.85-0.96 in Mabei, suggesting that the

Dongping gas field has the driest and most mature gas. In addition, $\delta^{13}C_{C1}$ can also reflect the hydrocarbon maturity because bonds with ^{12}C have a higher crack propensity than those with ^{13}C, endowing the ^{12}C isotope with a tendency to partition into hydrocarbons formed in the early stage of hydrocarbon generation. The gas dryness is consistent with the $\delta^{13}C_{C1}$ values in previous studies, ranging from -19.8‰ to -28.5‰ in Dongping, -35.3‰ to -28.4‰ in Mabei and -35.8‰ to -30.9‰ in Niudong (Tian et al., 2018; Zhou et al., 2016). The gas samples also include minor proportions of N_2 (1.15-8.87%), CO_2 (0.10-0.53%) and O_2 (0.02-0.19%).

4.2 Noble gases

He, Ne, Ar, Kr and Xe concentrations and isotopic ratios are given in Table 2.

Helium is more concentrated in Mabei and Dongping than in the Niudong gas field. The ^4He concentration ranges from 6.08 to 20.14×10^{-4} cm^3/cm^3 at standard temperature and pressure (STP) in the Mabei gas field, from 2.06 to 48.4×10^{-4} cm^3 STP/cm^3 in the Dongping gas field, and from 1.15 to 1.42×10^{-4} cm^3 STP/cm^3 in the Niudong gas field (Table 2). Helium isotopic ratios are 0.024-0.049 Ra in Mabei and 0.010-0.017 Ra in Niudong and Dongping, where Ra is the helium isotopic ratio in the atmosphere (Ra=1.4×10^{-6}, Mamyrin and Tolstikhin, 1984). Using a simple 2-endmember mixing model between sub-continental lithospheric mantle-like (6.1 Ra, Gautheron and Moreira, 2002) and upper crustal (0.008 Ra, Ballentine and Burnard, 2002) endmembers, the mantle contributions of helium are only 0.27-0.67% in Mabei and 0.03-0.15% in Dongping and Niudong, showing that helium in the three gas fields is mainly radiogenic.

The ^{20}Ne concentrations in the three gas fields range from 3.45×10^{-9} to 6.62×10^{-8} cm^3 STP/cm^3. Measured $^{20}Ne/^{22}Ne$ ratios vary between 8.75±0.14 and 9.96±0.16, showing minor deviations from the atmospheric value of 9.8. $^{21}Ne/^{22}Ne$ ratios vary from 0.0328±0.0009 to 0.0504±0.0012, slightly higher than the value of air (0.029). Neon isotope ratios can be explained

by mass fractionation and nucleogenic crustal ^{21}Ne and ^{22}Ne addition (Fig. 2). Nucleogenic ^{21}Ne and ^{22}Ne are mainly generated by ^{17}O, ^{18}O (α, n) ^{20}Ne, ^{21}Ne; ^{19}F (α, n) ^{22}Na (β^+) ^{22}Ne; and ^{19}F (α, p) ^{22}Ne in the crust, and the typical crustal endmember shown in fig.2 has a $^{21}Ne/^{22}Ne$ value of approximately 0.47 at the $^{20}Ne/^{22}Ne$ zero intercept (Kennedy et al., 1990, Ballentine and Burnard, 2002). Mabei and Dongping samples accumulate more nucleogenic ^{21}Ne than do Niudong samples.

The samples have ^{36}Ar concentrations ranging from 1.89 to 21.56×10^{-8} cm^3 STP/cm^3 and significantly different $^{40}Ar/^{36}Ar$ ratios. The $^{40}Ar/^{36}Ar$ ratios, ranging from 1726±36 to 2019±45 in Mabei, 883±16 to 2862±75 in Dongping, and 393±6 to 432±8 in Niudong, differ markedly from the atmospheric $^{40}Ar/^{36}Ar$ ratio of 298.56±0.31 (Lee et al., 2006). Due to the little mantle contribution indicated by the $^{3}He/^{4}He$ ratios in Section 4.2.1, the excess ^{40}Ar was likely generated by the radiogenic decay of potassium in the crust.

The ^{84}Kr concentrations range from 0.89 to 8.57×10^{-9} cm^3 STP/cm^3. The measured Kr isotopic ratios are indistinguishable from the atmospheric ratio. The $^{86}Kr/^{84}Kr$ ratio ranges between 0.301±0.0053 and 0.310±0.0058, similar to that of air (0.3035, Aregbe et al., 1996). Furthermore, the ^{130}Xe concentrations range from 2.08 to 12.00×10^{-11} cm^3 STP/cm^3, and the Xe isotopic ratios are also similar to those of air. Specifically, the $^{132}Xe/^{130}Xe$ ratios of 6.41±0.298 to 6.74±0.364 are similar to the atmospheric value (6.61, Pepin, 2000).

5. Discussion

5.1 Fractionation processes of atmosphere-derived noble gases

The noble gases, such as ^{20}Ne, ^{36}Ar, ^{84}Kr and ^{130}Xe, are predominantly derived from air, without significant contributions from radiogenic, nucleogenic or fissiogenic sources (Ballentine and Burnard, 2002). These gases originally dissolved into surface water under recharge conditions

and moved into the subsurface during aquifer recharge (Ballentine et al., 2002). The initial noble gas solubility in water increases with mass (Ne < Ar < Kr < Xe) and is controlled by the recharge conditions, such as temperature, salinity, and recharge elevation. When groundwater encounters hydrocarbons (e.g. during the hydrocarbon filling process), each of these elements is partioned into the oil or gas, and this process is controlled by Henry's law (Barry et al., 2017; Wen et al., 2017; Zhou et al., 2005). The characteristics of the atmospheric noble gases in these fluids are assumed to be conservative due to their inert chemical properties and limited subsurface sources. Therefore, atmosphere-derived noble gases (^{20}Ne, ^{36}Ar, ^{84}Kr and ^{130}Xe) and their ratios are used to model the history of multi-component (i.e., water, gas and oil) interactions within conventional and unconventional hydrocarbon systems (Ballentine et al., 1991; Barry et al., 2018; Byrne et al., 2018; Zhou et al., 2005).

We assume a temperature of 10ºC, a salinity of 0M NaCl, and an elevation of sea level as the recharge conditions for the three gas fields. The reservoir conditions of the Mabei, Dongping and Niudong gas fields differ significantly due to the various depths of the reservoirs, which are approximately 1000m, 3000m and 2000m, respectively (one exception is the Dongping 3 well with a depth of ~2000 m) (Zhou et al., 2016). The temperatures and pressures were calculated based on an average geothermal gradient of 3.4ºC/100 m and a pressure gradient of 13.3 bar/100m. Additionally, the groundwater salinity is assumed to be 2.02 M NaCl equivalent (~118 g/L on average). The oil density varies from 0.78-0.83 g/cm^3 and is assumed to be 0.80 g/cm^3 for simplification. The geothermal gradient, pressure gradient, groundwater salinity and oil density were measured by the Exploration and Development Research Institute, PetroChina Qinghai Oil Field Company. Henry's constants of the noble gases in water and oil were calculated from empirical equations under the above parameters and corrected with fugacity coefficients and

activity coefficients (Ballentine et al., 2002, Dymond and Smith, 1980, Smith and Kennedy, 1983). Henry's constants used in the following models are listed in Table 3.

5.1.1 Single-stage phase fractionation (gas-water equilibrium)

A single-stage phase equilibrium postulates that noble gases in the gas phase are directly degassed from groundwater during gas-groundwater equilibrium. Ne is more prone to degassing from groundwater than is Ar due to the lower solubility of Ne in water, meaning that the gas phase in equilibrium with water has a higher $^{20}Ne/^{36}Ar$ ratio than that in the water phase. Regardless of whether the system is closed or open, the highest $^{20}Ne/^{36}Ar$ ratio occurs in the first bubble equilibrated with groundwater under reservoir temperature and pressure (RTP) conditions, and these values are 0.310, 0.223 and 0.250 in the Mabei, Dongping and Niudong gas fields, respectively, except for the Dongping 3 well (0.250). The $^{20}Ne/^{36}Ar$ ratio in the gas phase decreases with an increase in the volume ratio of gas to water, which approaches 0 in an open system and becomes infinitely close to the value in the original air-saturated water (ASW) in a closed system (0.143). We observed that the measured $^{20}Ne/^{36}Ar$ ratios in Niudong gas (0.120-0.133) were lower than the minimum ratio of 0.143 in the gas phase in a closed system, which can only be explained by gas-water fractionation in an open system.

The influence of the variation in recharge conditions on the models have been considered. 1) When the salinity of recharge water is higher than the assumed value in this study (0 M NaCl), the initial $^{20}Ne/^{36}Ar$ ratio in ASW and the lowest $^{20}Ne/^{36}Ar$ ratio equilibrated into gas phase in a closed system are higher than 0.143, which is higher than part of the measured $^{20}Ne/^{36}Ar$ ratio (0.120-0.291), therefore, only the open system fractionation model could explain the data. 2) As the recharge temperature decreased gradually, a recharge temperature of 0 ºC would result in a minimum $^{20}Ne/^{36}Ar$ ratio partitioning into the gas phase in a closed system of 0.122, which could

explain the measured data (0.120±0.002 - 0.291±0.006) within errors. However, at the recharge temperature of 0 °C, the highest $^{20}Ne/^{36}Ar$ ratio that could occur in the gas phases in Mabei both in a closed and an open system decreases to 0.250, which could not explain the measured values in this area (0.210-0.291). Therefore, a recharge temperature of 0 °C could not be used in the modelling. Based on the considerations above, a recharge temperature of 10 °C was used together with the Rayleigh fractionation law to model the gas-water equilibrium process in an open system at the Qaidam Basin (Ballentine et al., 2002 and references therein):

$$\left({}^{20}Ne/{}^{36}Ar\right)_{water} = \left({}^{20}Ne/{}^{36}Ar\right)_{ASW} \mathrm{f}^{\alpha-1} \quad (1)$$

$$\alpha = \frac{K^{d}_{Ne(water)}}{K^{d}_{Ar(water)}} \quad (2)$$

where $\left({}^{20}Ne/{}^{36}Ar\right)_{water}$ is the $^{20}Ne/^{36}Ar$ ratio in the groundwater phase after equilibrium; $\left({}^{20}Ne/{}^{36}Ar\right)_{ASW}$ is the $^{20}Ne/^{36}Ar$ ratio in the original air-saturated water (ASW); f is the fraction of ^{36}Ar remaining in the groundwater phase, and α is the fractionation coefficient for the gas/groundwater system. $K^{d}_{Ne(water)}$ and $K^{d}_{Ar(water)}$ are dimensionless Henry's constants of Ne and Ar in groundwater. As an infinitesimally small amount of gas equilibrates with groundwater, the $^{20}Ne/^{36}Ar$ ratio in the gas phase after equilibrium $\left({}^{20}Ne/{}^{36}Ar\right)_{gas}$ is given by:

$$\left({}^{20}Ne/{}^{36}Ar\right)_{gas} = \left({}^{20}Ne/{}^{36}Ar\right)_{water} \alpha \quad (3)$$

Based on the measured $^{20}Ne/^{36}Ar$ ratio in the gas phase, the ^{36}Ar remaining in the groundwater phase (f) can be calculated by Equations (1)-(3). Then, the ^{36}Ar concentration in the gas phase $({}^{36}Ar)_{gas}$ (m^3/m^3) can be calculated as follows:

$$\left({}^{36}Ar\right)_{\mathrm{gas}} = ({}^{36}Ar)_{ASW} \mathrm{f}\, K^{d}_{Ar(water)}/Z \quad (4)$$

where $({}^{36}Ar)_{ASW}$ is the ^{36}Ar concentration in ASW (m^3 STP/m^3); the other parameters are the same as those in Equations (1)-(3). Z is the compression factor that converts noble gas concentrations from STP (273.15 K at 1 bar) to RTP and is given by Barry et al. (2016):

$$Z = 273.15 P_R / T_R \quad (5)$$

where P_R is the reservoir pressure in atm and T_R is the reservoir temperature. Based on the measured $^{20}Ne/^{36}Ar$ ratio, the calculated ^{36}Ar concentrations in the gas phase of Mabei range from 5.56 to 7.35×10^{-7} cm^3 STP/cm^3, which is 6.9-9.2 times the measured ^{36}Ar concentrations in natural gas. Similarly, the calculated ^{36}Ar concentrations in the gas phase are 2.8-11.0 and 1.6-3.3 times the measured ^{36}Ar concentrations in the Dongping and Niudong gas fields, respectively. This suggests that the gas-groundwater fractionation in an open system cannot explain the measured ^{20}Ne and ^{36}Ar concentrations. Therefore, there is likely another process that can dilute the air-derived noble gases (ADGs) before or after gas-water equilibration. In addition, the $^{20}Ne/^{36}Ar$ ratio in the Dongping 3 well (0.287) is higher than the modelling maximum value (0.250) in the gas phase at Dongping RTP, indicating that single-stage gas-groundwater fractionation cannot explain the measured ADGs characteristics.

5.1.2 Two-stage phase fractionation (oil-modified groundwater-exsolution)

Based on the theory of hydrocarbon generation, all types of hydrocarbon source rocks, including the type II-III in the North Qaidam Basin, can produce both oil and gas phases (Yang et al., 1985). Furthermore, long-chain hydrocarbons (oil) are generated in an earlier stage than methane (Tissot and Welte, 1984). Because the Mabei and Niudong gas fields are distributed in oil and gas areas and Mabei is near the Nanbaxian oil field (Fig. 1a), we sought to characterize the noble gas in the natural gas by oil-groundwater fractionation followed by gas-groundwater equilibrium, similar to the oil-modified groundwater exsolution (OMG-E) model in Zhou et al. (2012) and the double distillation model in Battani et al. (2000). In this work, we follow the OMG-E model, which suggests that an oil phase is equilibrated with the groundwater during the early stage of hydrocarbon generation, this process is then followed by subsequent equilibrium between

gas and the fractionated groundwater.

Involvement of the oil phase can explain two discrepancies in the single-stage gas-groundwater equilibration. 1) The measured ^{20}Ne and ^{36}Ar concentrations are lower than the predicted concentrations. Because noble gases are more soluble in oil than in water, the equilibration between an oil phase and groundwater results in the transfer of noble gases from the groundwater to the oil. Therefore, the process reduces the noble gas concentrations in the groundwater before gas-groundwater fractionation, resulting in less noble gas degassing into the gas phase in the gas-groundwater equilibration process. 2) The measured $^{20}Ne/^{36}Ar$ ratio in the Dongping 3 sample is higher than the predicted maximum value. Relative to Ne, Ar is more soluble in oil than in water (Ballentine et al., 2002); therefore, the equilibration between oil phase and groundwater phase increases the $^{20}Ne/^{36}Ar$ ratio in the water phase and increases the $^{20}Ne/^{36}Ar$ ratio fractionation limit in the gas phase in contact with the water phase.

Since hydrocarbon source rocks are distributed in depressions rather than under the reservoirs in the Mabei and Dongping areas, the gas and oil must migrate laterally and vertically for several kilometres from adjacent depressions (Fig. 1). The long migration distance supported our model that the equilibrium among gas, oil and water proceeds in an open system from initial stage for both oil-water and gas-water systems. The two stages of Rayleigh oil-water fractionation and Rayleigh gas-water fractionation in an open system are described by the following equations):

$$\left({}^{20}Ne/{}^{36}Ar\right)_{gas} = \left({}^{20}Ne/{}^{36}Ar\right)_{ASW} f_1^{(\alpha_1-1)} f_2^{(\alpha_2-1)} \alpha_2 \quad (6)$$

$$\left({}^{36}Ar\right)_{gas} = \left({}^{36}Ar\right)_{ASW} f_1 f_2 K^d_{Ar(water)}/Z \quad (7)$$

where $\left({}^{20}Ne/{}^{36}Ar\right)_{gas}$ and $\left({}^{20}Ne/{}^{36}Ar\right)_{ASW}$ are the $^{20}Ne/^{36}Ar$ ratios in the gas phase and original groundwater (ASW), respectively; f_1 and f_2 are the fractions of ^{36}Ar remaining in the groundwater phase after oil-water and after gas-water equilibrium, respectively; and Z is the

compression factor given by Equation (5). α_1 and α_2 are the Ne-Ar fractionation coefficients for the oil/water and gas/water systems, given by:

$$\alpha_1 = \frac{K^m_{Ne(water)} K^m_{Ar(oil)}}{K^m_{Ne(oil)}\, K^m_{Ar(water)}} \quad (8); \quad \alpha_2 = \frac{K^m_{Ne(water)}}{K^m_{Ar(water)}} \quad (9)$$

where the superscript m means that Henry's constant (K) is expressed in the unit of atm kg/mol. The modelling results (Fig. 3) suggest that the data from the Mabei and Niudong gas fields show a similar trend to that of the modelled line and fit the gas-groundwater fractionation in an open system well.

However, the data from Dongping are not consistent with the model line in an open system (not shown in Fig.3); therefore, we also modelled the situation considering gas-water fractionation in a closed system to figure out the best explanation for data in Dongping area. We still assume that the oil-water fractionation proceeds in an open system due to the long-distance migration of hydrocarbon. Oil-water fractionation in an open system and gas-water fractionation in a closed system are described by the following equations:

$$\left({}^{20}Ne/{}^{36}Ar\right)_{gas} = \left({}^{20}Ne/{}^{36}Ar\right)_{ASW} f_1^{(\alpha_1-1)\frac{\frac{V_{gas}}{V_{water}}+\frac{1}{K^d_{Ar(water)}}}{\frac{V_{gas}}{V_{water}}+\frac{1}{K^d_{Ne(water)}}}} \quad (10)$$

$$\left({}^{36}Ar\right)_{gas} = \left({}^{36}Ar\right)_{ASW} f_1 \left(\frac{V_{gas}}{V_{water}} + \frac{1}{K^d_{Ar(water)}}\right)^{-1} / Z \quad (11)$$

where V_{gas}/V_{water} is the volume ratio of gas to water under RTP and all other parameters are the same as those in the above equations. Solving Equations (10) and (11), we can obtain the f_1 and V_{gas}/V_{water} values. Since the Dongping 3 well has a reservoir depth of approximately 2000 m, which is different from the other two wells in this area (3000 m), the Dongping 3 well is modelled separately. The modelling results show that the data from Dongping are well explained by the model of oil-water fractionation in an open system and gas-groundwater fractionation in a closed system (Fig. 3).

Although Fig. 3 provides a good explanation for the measured data, we also investigated other modelling situations to test whether the measured Mabei and Niudong data could fit the fractionation model that was used to explain the Dongping data. Our results showed that this model is less consistent with the Mabei data compared to the model line in an open system. It also cannot explain the Niudong data since the data are distributed below the boundary line (the gas-water equilibrium line when the V_{oil}/V_{water} ratio equals 0). Therefore, we use the model of oil-water and gas-water fractionation both in an open system to explain the Mabei and Niudong data and the model of oil-water fractionation model in an open system and gas-water in a closed system to interpret the measured Dongping values.

5.1.3 Volume ratio of oil, gas and groundwater

The relative oil, gas and groundwater amounts in the system can be quantified based on the models discussed in previous section. For oil-water and gas-water Rayleigh fractionation model in an open system, step-wise oil-water and gas-water equilibration can approximate Rayleigh fractionation if the volume ratios V_{oil}/V_{water} and V_{gas}/V_{water} are low in each stage (Zhou et al., 2005). Equations for V_{oil}/V_{water} and V_{gas}/V_{water} in a single equilibration process between oil and water phases at STP are given by Battani et al. (2000) and Ballentine et al. (2002), respectively:

$$\frac{V_{oil}}{V_{water}} = \frac{\rho_{water} K^{m}_{Ar(oil)}}{\rho_{oil} K^{m}_{Ar(water)}} \left(\frac{1-f_1}{f_1}\right) \quad (12)$$

$$\frac{V_{gas}}{V_{water}} = \frac{Z(1-f_2)}{f_2 K^{d}_{Ar(water)}} \quad (13)$$

where V_{oil}, V_{gas}, and V_{water} are the volumes of oil, gas and groundwater, respectively, in the oil-gas-water system under RTP and ρ_{oil} and ρ_{water} are the densities of oil and water, which are 0.80 g/cm^3 and 1 g/cm^3, respectively. The other parameters are the same as those in the equations above. We assume that a small volume of oil (gas) equilibrates with the groundwater in each individual stage ($V_{oil}/V_{water}=V_{gas}/V_{water}=3\times10^{-5}$, Zhou et al., 2005); then, the fraction of ^{36}Ar remaining in the

groundwater phase in each step ($f_{1single}$ and $f_{2single}$) can be calculated by Equations 12 and 13. Furthermore, the numbers of individual stages of oil/water (n_1) and gas/water (n_2) equilibration can be calculated by $f_1=f_{1single}$^n_1 and $f_2=f_{2single}$^n_2. The sum of the volume ratios of oil (gas) to water defines the total volume ratio of oil (gas) to water involved in the oil-water and gas-water fractionation processes.

For the model of oil-water fractionation in an open system and gas-water fractionation in a closed system, the V_{gas}/V_{water} ratio at RTP can be obtained by solving Eqs. (10) and (11), and the V_{gas}/V_{water} ratio at STP can further be obtained through multiplying by the compression factor Z. The V_{oil}/V_{water} ratio in this model can also be calculated by Eq. (12). The results are listed in Table 4.

The ratios among the gas, oil and groundwater in the OMG-E model agree well with the geological context, which is independent evidence for the credibility of the model. The modelled V_{gas}/V_{water} ratio of the Dongping 3 well (0.71) is lower than the values of other wells in the three gas fields (1.09-39.15), consistent with the lower gas production and higher water production in the Dongping 3 area (Li et al., 2014). In addition, the model results reveal that the V_{gas}/V_{oil} ratios range from 75.97 to 151.48 in Niudong and from 292.97 to 1081.28 in Dongping (except for Dongping 3=17.20), while the ratios vary between 9.93 and 13.36 in Mabei. These ratios agree well with the oil reservoirs discovered in the Mabei gas field (Fig. 1b) and the lower gas dryness of Mabei (0.76-0.98) compared to those of Niudong (0.89-0.90) and Dongping (0.95-0.99) (Tian et al., 2018; Zhou et al., 2016 and this study). These results suggest that Mabei is the most oil-rich area among these three gas fields. Although some gas samples in Mabei are characterized by high coefficients of gas dryness (up to 0.98), these findings are not contradictory to the modelled low V_{gas}/V_{oil} ratio in Mabei because pockets of oil could fail to be preserved if oil migration occurred

earlier than the development of the trapping structure.

Assuming the groundwater quantities in the three gas fields are similar, the V_{oil}/V_{water} and V_{gas}/V_{water} ratios can provide a means to evaluate the production of gas and oil in the gas fields. Except for that of Dongping 3, the V_{oil}/V_{water} ratios indicate that the generated oil quantity in Mabei is approximately 2.9 and 3.9 times of those in the Niudong and Dongping gas fields, respectively. Similarly, the V_{gas}/V_{water} ratios show that the generated gas amount in Mabei is only 36.2% and 5.7% of those in Niudong and Dongping. Therefore, the Dongping area is the most favourable area for gas accumulation, especially the No. 5 block, where the Dongping 171 well is located.

5.1.4 Heavy noble gas enrichments

The heavy noble gases (Kr and Xe) in the samples are characterized by air-like isotopic compositions, lacking the accumulation of fissiogenic Kr and Xe. Based on the OMG-E model used in this study, the calculated Kr and Xe concentrations in the gas phase partitioned from ASW are only 16-67% and 0.14-30% of the measured values. It is uncertain whether the released Kr and Xe equilibrated with deep meteoric formation waters before partitioning into the oil and gas phase, which complicates the explanation of the measured Kr and Xe data (Barry et al., 2018). Therefore, the solubility-controlled fractionation model cannot reasonably explain the measured data. Because heavy noble gases are preferentially absorbed on organic sediments and siliceous fossils relative to He, Ne and Ar (Podosek et al., 1981, Matsuda and Nagao, 1986), when hydrocarbons are generated, heavy noble gases are released and migrate into the fluid system, providing an additional contribution to the heavy noble gas concentrations other than that provided by ASW (Barry et al., 2016; Torgersen and Kennedy, 1999; Zhou et al., 2005). Excess heavy noble gas enrichment has been demonstrated to be a common phenomenon in coalbed methane, gas fields, oil fields, shale gas systems, and CO_2 gas fields (Barry et al., 2018; Gilfillan et al., 2008; Wen et

al., 2017; Zhou et al., 2005).

5.2 Helium accumulation process

Commercial helium is often exploited from CH_4 gas fields; however, helium concentrations vary in a big range among gas fields globally (Ballentine and Lollar, 2002; Boreham et al., 2018 and references therein). This fact gives rise to an interesting question: what are the critical processes controlling helium accumulation in natural gas fields? In this work, we aim to understand this question based on the example of the gas fields in the North Qaidam Basin.

5.2.1 Relationship between helium and groundwater

The $^{3}He/^{4}He$ ratios (0.01-0.05 Ra) in the North Qaidam Basin indicate that helium in the gas fields is mainly derived from the radiogenic decay of uranium and thorium in the crust. ^{20}Ne in natural gas is derived from ASW due to lack of other sources in the crust and mantle (Ballentine and Burnard, 2002). Therefore, the relationship between ^{4}He and ^{20}Ne can reflect the influence of groundwater on helium accumulation. As shown in Fig. 4, the linear relationship between ^{4}He and ^{20}Ne indicates that ^{4}He was transported together with ^{20}Ne by groundwater before migrating into the oil or gas phase. Because He and Ne have similar solubilities in oil and water, solubility-controlled fractionation has little effect on the $^{4}He/^{20}Ne$ ratio. Therefore, the $^{4}He/^{20}Ne$ ratio is only controlled by the ratio between quantity of the involved groundwater to the amount of helium production. A similar relationship between ^{4}He and ^{20}Ne is also shown in the Hugoton-Panhandle gas field (Ballentine and Lollar, 2002), southwestern Kansas (Danabalan, 2017), and the Weihe Basin, China (Zhang et al., 2019).

In addition, taking the Mabei gas field as an example, the solubility of He under reservoir conditions is approximately 0.724 cm^3STP/g, which is much higher than the calculated initial ^{4}He concentrations in groundwater (9.18-13.88×10^{-3} cm^3STP/cm^3 H_2O, see Section 5.2.2). This

suggests that helium should have dissolved in groundwater before equilibrating with the oil and gas phases.

5.2.2 Initial ^{4}He concentrations in the groundwater and dilution of helium by CH_4 in the reservoir

The initial concentration of ^{4}He (as well as ^{21}Ne* and ^{40}Ar*) in groundwater before oil-gas-water interaction can be estimated based on the measured ^{4}He (or ^{21}Ne*, ^{40}Ar*) concentration in the gas phase and the fractionation process. Taking ^{4}He as an example, the initial ^{4}He concentration in groundwater in the Mabei and Niudong gas fields (Rayleigh oil-water fractionation and Rayleigh gas-water fractionation) is given by:

$$\left({}^4He\right)_{initial} = \frac{\left({}^4He\right)_{gas} Z}{K^d_{He(water)} f_1^{\alpha'_1} f_2^{\alpha'_2}} \quad (14)$$

$$\alpha'_1 = \frac{K^m_{He(water)} K^m_{Ar(oil)}}{K^m_{He(oil)}\, K^m_{Ar(water)}}; (15) \quad \alpha'_2 = \frac{K^m_{He(water)}}{K^m_{Ar(water)}} \quad (16)$$

The initial ^{4}He concentration in the groundwater in the Dongping gas field (open oil-water fractionation and closed gas-water fractionation) is given by:

$$\left({}^4He\right)_{initial} = \frac{\left({}^4He\right)_{gas} Z}{f_1^{\alpha'_1}} \left(\frac{V_{gas}}{V_{water}} + \frac{1}{K^d_{He(water)}}\right) \quad (17)$$

where the parameters in Equations (14)-(17) are the same as those in Equations (6), (7), (12), and (13). α'_1 and α'_2 are the He-Ar fractionation coefficients for the oil/water and gas/water systems, respectively. The results show that He was more concentrated in the groundwater of Mabei and Dongping (0.92-1.40×10^{-2} cm^3 ^{4}He STP/cm^3 H_2O) than in Niudong (2.07-3.21×10^{-3} cm^3 ^{4}He STP/cm^3 H_2O) (Table 4). These values agree with the higher ^{40}Ar/^{36}Ar ratios in the Mabei and Dongping fields (883-2862) than those in the Niudong field (393-432). ^{21}Ne* and ^{40}Ar* have similar patterns as ^{4}He, which are discussed in Section 5.3. The reason for the lower initial ^{4}He concentration in the groundwater in Niudong is discussed in Section 5.2.3. Here, we focus on the

variation in the ^{4}He concentrations in the gas and groundwater in Mabei and Dongping, which can be measured by the coefficient of variation (C.V.). This parameter is defined as follows:

$$\mathrm{C.V.} = \frac{\sigma}{\mu} \qquad (18)$$

where σ is the standard deviation and μ is the mean value of ^{4}He concentrations in gas or groundwater phase. Results suggest that the C.V.s of ^{4}He contents in gas phases in Mabei and Dongping are 0.39 and 1.10 respectively, higher than those of initial ^{4}He concentrations in groundwater in the two gas fields (C.V.=0.17 and 0.27, respectively). It suggests, despite the large variation in the measured ^{4}He concentrations in the gas phase in Mabei and Dongping, the estimated initial ^{4}He concentrations in groundwater vary to a less extent. The ^{4}He variation in the gas phase in Mabei and Dongping can be explained by different CH_4 volumes present in the system, i.e., CH_4 reduces the ^{4}He concentrations in the gas phase. The major gases (e.g., CH_4) have a significant dilution effect on ^{4}He and other noble gases partitioned into the gas phase in a similar fashion to the dilution effect of CH_4 on ^{36}Ar in the shale gas system (Byrne et al., 2018).

5.2.3 Accumulation of He in groundwater

Helium is mainly produced by the radiogenic decay of ^{235}U, ^{238}U and ^{232}Th in rocks. Subsequently, several mechanisms control the release of helium from rock and minerals (e.g., recoil, diffusive loss, fracturing and mineral transformation). Thus, the He accumulation in groundwater is contributed by in situ production and an external flux (Barry et al., 2017; Torgersen and Clarke, 1985). The in situ accumulation and external flux of ^{4}He in groundwater are given by Torgersen (1980) and Zhou and Ballentine (2006) respectively:

$$\left[\,^4He\right]^{groundwater}_{in\ situ\ production} = \frac{\rho \Lambda J_4 (1-\varphi)}{\varphi} t \qquad (19)$$

$$\left[\,^4He\right]^{groundwater}_{external\ flux} = \frac{J_4 \rho H}{\varphi h} t \qquad (20)$$

where ρ is the density of porous rock in g/cm^3; Λ is the ^{4}He transfer efficiency from the rock matrix to the groundwater, which is assumed to be 1; φ is the rock porosity; and t is the groundwater residence time in years. Additionally, H is the average thickness of the helium source rock in km; h is the aquifer thickness in km; and J_4 is the radioactive production of ^{4}He in groundwater in cm^3 STP ^{4}He/g_{rock} year, given by Craig and Lupton (1976):

$$J_4 = 0.2355 \times 10^{-12}\ [U]\{1 + 0.123([Th]/[U] - 4\} \quad (21)$$

[U] and [Th] are the U and Th concentrations, respectively, in rocks in ppm. Based on Equations (19) and (21), we assume that ^{4}He in groundwater is accumulated between the deposition of the Eocene layers (56 Ma) and the beginning of the hydrocarbon filling process (23 Ma); then, the maximum in situ ^{4}He production in groundwater is calculated to be 7.80-16.4 $\times 10^{-4}$ cm^3 ^{4}He STP/cm^3 H_2O. The value is one order of magnitude lower than the calculated initial ^{4}He concentration in groundwater; therefore, the contribution of an external ^{4}He flux from the crust should be considered in this case.

An external ^{4}He flux from the entire crust (upper crust and lower crust) is used to calculate the time needed for groundwater to accumulate the observed concentration of helium. We choose the average U and Th concentrations of acidic rock (3.5 and 18 ppm, respectively, Vinogradov and Ryabchikov, 1962) as the values of the upper crust because of the granitic-metamorphic basement. The U and Th concentrations of the lower crust are taken to be 0.28 and 1.07ppm respectively (Zhou and Ballentine, 2006). Results show that the ^{4}He accumulation period in Mabei is the longest (1.84-2.78Ma), followed by Dongping (1.07-2.11Ma) and Niudong (0.31-0.35Ma). This suggests that the groundwater in Niudong is younger than that in Mabei and Dongping, which is why the calculated initial ^{4}He concentrations in groundwater in the former are lower than those in the latter.

5.2.4 Insignificant contribution of ^{4}He to the gas reservoirs after their formation

The ^{4}He contribution to the gas reservoir after gas filling can be derived from the external flux and in situ production. Since groundwater is widespread in the crust and ^{4}He in the gas reservoir has a close relationship with groundwater (see Section 5.2.1), the external ^{4}He flux from the deep crust should dissolve into groundwater in the first stage. Because it is less possible for the gas reservoir to equilibrate with large-scale groundwater after hydrocarbon filling, in which some ^{4}He is partitioned into the gas reservoir from the groundwater phase, the external ^{4}He flux contribution after gas filling can be ignored. The in-situ production of ^{4}He (cm^3 STP/cm^3) after the formation of reservoir can be calculated using the following equation after Byrne et al. (2018):

$$[\,^4He]_{in-situ}^{gas} = \frac{\rho \Lambda J_4 (1-\varphi) t}{\varphi Z} \quad (22)$$

where Z is the compression factor of CH_4 under reservoir pressure and temperature conditions given by Equation 5 and accounts for the dilution of produced ^{4}He by pressurized CH_4. The other parameters are the same as those in Equations (19)-(21). Results show that the accumulated ^{4}He concentration in the gas reservoir after the hydrocarbon filling (~2.58 Myr in Dongping and Niudong area, Cao et al., 2013) is only (1.70-6.18)×10^{-7} cm^3 /cm^3, which is 3-4 orders of magnitude less than the measured ^{4}He concentration in the gas phase. This observation suggests that the contribution of in situ ^{4}He production to the reservoir after hydrocarbon filling is negligible. The relationship between ^{4}He and ^{20}Ne (Fig. 4) indicates that the majority of ^{4}He is migrated from groundwater to the gas phase along with ^{20}Ne rather than directly from the rocks to the gas phase, which further demonstrates that there was little ^{4}He contribution to the gas reservoir after hydrocarbon filling.

5.2.5 Other crust-derived noble gases

In addition to ^{4}He, ^{21}Ne and ^{40}Ar also have significant contributions from the crust. The explicit crust-derived components for Ne and Ar ($^{21}Ne^{*}$ and $^{40}Ar^{*}$) are corrected for atmospheric contributions by assuming a pure atmospheric source for ^{20}Ne and ^{36}Ar. The in situ production ratios of $^{4}He/^{40}Ar^{*}$ and $^{21}Ne^{*}/^{40}Ar^{*}$ are calculated to be 7.5 and $3.19\times10^{-7,}$ respectively, on the basis of average U, Th, and K concentrations of 3.5 ppm, 18 ppm, and 3.34%, respectively, in acidic rock (Vinogradov and Ryabchikov, 1962) and an average crustal $^{4}He/^{21}Ne^{*}$ ratio of 2.33×10^{7} (Ballentine and Burnard, 2002). As He and Ne have similar solubilities in water, the linear relationship between the measured $^{4}He/^{40}Ar^{*}$ and $^{21}Ne^{*}/^{40}Ar^{*}$ values (Fig. 6a) indicates that the scattered $^{4}He/^{40}Ar$ ratios are controlled by solubility-dependent fractionation. The crust derived noble gas concentrations in the initial groundwater are calculated based on the OMG-E model. Results (Fig. 6b) show that there are two sources for ^{4}He, $^{21}Ne^{*}$ and $^{40}Ar^{*}$: the first source features low $^{4}He/^{40}Ar^{*}$ ratios (4.16-6.15) and low $^{21}Ne^{*}/^{40}Ar^{*}$ ratios ($1.30\text{-}2.21\times10^{-7}$), which are slightly lower than the in situ production ratios; the second source has high $^{4}He/^{40}Ar^{*}$ ratios (14.4-17.9) and low $^{21}Ne^{*}/^{40}Ar^{*}$ ratios ($4.31\text{-}6.90\times10^{-7}$). Although the $^{21}Ne^{*}/^{40}Ar^{*}$ ratios in the second group have large variations, the values are consistent within error. This suggests that the scattered $^{4}He/^{40}Ar^{*}$ and $^{21}Ne^{*}/^{40}Ar^{*}$ values in Fig. 6a are likely evolved from the two sources in Fig. 6b.

A relationship between ^{4}He and $^{21}Ne^{*}$ (the slopes of the fitting lines in Fig. 6) is expected because ^{4}He is produced by the radiogenic decay of U and Th and Ne is generated by nucleogenic routes, which are controlled by the amount of α-particles, which in turn is controlled by U and Th concentrations. The different $^{4}He/^{40}Ar^{*}$ ratios may be caused by the local elemental ratio between U, Th and K or the preferential release of He compared to Ar (Ballentine and Burnard, 2002).

5.3 He accumulation processes in the North Qaidam Basin

Based on the findings in previous sections, we summarized the helium accumulation processes in the North Qaidam Basin in the following 5 steps (Fig. 5).

(1) Helium in the North Qaidam Basin is mainly derived from crust and generated by radiogenic decay of U and Th, which are suggested by the $^{3}He/^{4}He$ ratios of 0.011-0.049 Ra.

(2) Majority of the produced helium is released and preserved in groundwater. The close relationship between ^{4}He and ^{20}Ne suggests that the majority of ^{4}He in gas reservoir is exsolved from groundwater to the gas phase along with ^{20}Ne rather than directly migrated from the rocks to the gas phase.

(3) Helium concentrations in the groundwater increase with the residence time of the water. The initial ^{4}He contents in the groundwater in Mabei and Dongping (2.07-3.21×10^{-3} cm^3 STP/cm^3) are much higher than those in Niudong (0.92-1.40×10^{-2} cm^3 STP/cm^3), which takes 1.07-2.78Ma and 0.31-0.35Ma, respectively to accumulate when assuming a ^{4}He flux from the entire crust. The younger groundwater in Niudong gas field than those in Mabei and Dongping gas fields cause the lower He concentrations in the former than the latter.

(4) Helium in the groundwater is degassed by oil and gas and subsequently transported into reservoir along with the hydrocarbons. In the North Qaidam Basin, oil and gas phases subsequently contact with groundwater and partition helium in groundwater into the hydrocarbon phases (oil-modified groundwater-exsolution model). In this process, different volumes of oil, gas and groundwater were involved and caused various ^{4}He concentrations in gas phases (C.V. = 0.39 and 1.10 in Mabei and Dongping) compared to those in initial groundwater (C.V. = 0.17 and 0.27 in Mabei and Dongping). Dongping 171 produces a higher gas quantity (V_{gas}/V_{water}=39.15) and a lower ^{4}He concentration (($^{4}He)_{gas}$=0.021%) compared to Dongping 3 (V_{gas}/V_{water} = 0.71 and ($^{4}He)_{gas}$ = 0.484%), suggesting that, although the existence of gas phase is a necessary condition

to partition helium out of groundwater, a large amount of hydrocarbons can dilute the helium concentration in the gas phase, which reduces the commercial value of the reservoir for producing helium gas.

(5) There is insignificant helium contributed to the gas reservoir after the reservoir formation due to the absence of large-scale gas-water contact after hydrocarbon filling.

In summary, a gas field associated with old groundwater systems and filled by moderate amount of hydrocarbon gases are more likely to accumulate high concentrations and amounts of helium for exploration purposes.

6. Conclusions

We present high-precision noble gas (He, Ne, Ar, Kr and Xe) isotope and abundance data as well as major gas compositional data from 10 producing wells in the Mabei, Dongping and Niudong gas fields in the North Qaidam Basin, China. These data are used to quantifiably investigate helium accumulation mechanism and hydrocarbon charging processes in a water-oil-gas system. Results can provide insights and guidance in exploring helium as a strategic resource.

$^{3}He/^{4}He$ ratios show that there is little contribution from the mantle source, indicating that the majority of noble gases in the gas reservoirs are derived from ASW and the crust. The ASW-derived noble gases (^{20}Ne, ^{36}Ar, ^{84}Kr and ^{130}Xe) can be accounted for by the OMG-E model with excess heavy noble gases. The data from Mabei and Niudong can be interpreted as open-system fractionation between oil and water followed by gas and water fractionation. The Dongping data can be explained by equilibration in an open oil/water system followed by a closed gas/water system. The calculated V_{oil}/V_{water} ratios and V_{gas}/V_{water} ratios suggest that Mabei is the most oil-rich area and Dongping has the driest natural gas, which is consistent with the geological context

and supports our fractionation model.

The linear relationship between ^{4}He and ^{20}Ne indicates that ^{4}He is dissolved into the groundwater and mixed with ^{20}Ne before in contact with the oil or gas phase. The estimated initial ^{4}He concentrations in the groundwater are less variable (C.V.=0.39 and 1.10 for Mabei and Dongping, respectively) than the measured ^{4}He concentrations in the gas phase (C.V.=0.17 and 0.27, respectively), indicating that CH_4 has a significant dilution effect on ^{4}He and other noble gases partitioned into the gas phase. The groundwater residence times are calculated to be 0.31-2.78 Myr assuming an external ^{4}He flux derived from the entire crust. The groundwater in Niudong is younger than that in Mabei and Dongping, which is consistent with the lower He concentrations in the Niudong gas field than those in the Mabei and Dongping gas fields. The calculation based on He production suggests that little ^{4}He was contributed to the gas reservoir after filling of the hydrocarbons in the reservoir. Based on the OMG-E model, the $^{4}He/^{40}Ar^{*}$ and $^{21}Ne^{*}/^{40}Ar^{*}$ ratios in the gas phase are derived from two sources, which are ultimately controlled by the in situ production ratio.

The helium accumulation process can be summarised into 5 steps. 1) Helium is generated by radiogenic decay of U and Th in the crust. 2) Majority of helium is released and dissolved into groundwater present in rock fractures. 3) Groundwater with a long residence time can accumulate high amount of He. 4) Helium in the groundwater partitions into oil and gas and is subsequently transported into the hydrocarbon reservoir, where hydrocarbons have a dilution effect on the helium concentration in the gas phase. 5) There is insignificant contribution of He to the reservoir after the formation of gas reservoir. It is more likely to succeed in helium exploration at gas fields associated with old groundwater systems and moderate hydrocarbon reserve.

Acknowledgments

This research has been supported by the National Natural Science Foundation in China (No. 41572131). We thank China Scholarship Council for supporting the collaborative work with Lancaster University and the University of Manchester. We acknowledge the team No. 105, Qinghai Bureau of Coal Geology, for assistance during sampling work. Editorial handling by Prof. Balz Kamber and helpful comments from two anonymous reviewers, which have greatly improved this work, are much appreciated.

References

Aregbe, Y., Valkiers, S., Mayer, K., De Bièvre, P., 1996. Comparative isotopic measurements on xenon and krypton. Int. J. Mass Spectrom. Ion Processes, 153(1): L1-L5.

Ballentine, C., 2017. Helium in crisis, Chemistry World, Cambridge. URL: https://www.chemistryworld.com/opinion/helium-in-crisis/3007152.article

Ballentine, C., O'nions, R., Oxburgh, E., Horvath, F., Deak, J., 1991. Rare gas constraints on hydrocarbon accumulation, crustal degassing and groundwater flow in the Pannonian Basin. Earth Planet. Sci. Lett. 105(1-3): 229-246.

Ballentine, C.J., Burgess, R., Marty, B., 2002. Tracing fluid origin, transport and interaction in the crust. Rev. Mineral. Geochem. 47(1): 539-614.

Ballentine, C.J., Burnard, P.G., 2002. Production, Release and Transport of Noble Gases in the Continental Crust. Rev. Mineral. Geochem. 47(1): 481-538.

Ballentine, C.J., Lollar, B.S., 2002. Regional groundwater focusing of nitrogen and noble gases into the Hugoton-Panhandle giant gas field, USA. Geochim. Cosmochim. Acta 66(14): 2483-2497.

Bare, S.R., Lilly, M., Chermak, J., Eggert, R., Halperin, W., Hannahs, W., Hayes, S., Hendrich, M., Hurd, A., Osofsky, M., Tway, C., 2016. Responding to the U.S. research community's liquid helium crisis, Washington, D.C..

Barry, P.H., Kulongoski, J.T., Landon, M.K., Tyne, R.L., Gillespie, J.M., Stephens, M.J., Hillegonds, D.J., Byrne, D.J., Ballentine, C.J., 2018. Tracing enhanced oil recovery signatures in casing gases from the Lost Hills oil field using noble gases. Earth Planet. Sci. Lett. 496: 57-67.

Barry P.H., Lawson M., Meurer W.P., Danabalan D., Byrne D.J., Mabry J.C. and Ballentine C.J., 2017. Determining fluid migration and isolation times in multiphase crustal domains using noble gases. Geology 45, 775-778.

Barry, P.H., Lawson, M., Meurer, W.P., Danabalan D., Byrne, D.J., Mabry, J.C., Ballentine, C.J., 2016. Noble gases solubility models of hydrocarbon charge mechanism in the Sleipner Vest gas field. Geochim. Cosmochim. Acta 194: 291-309.

Battani, A., Sarda, P., Prinzhofer, A., 2000. Basin scale natural gas source, migration and trapping traced by noble gases and major elements: the Pakistan Indus basin. Earth Planet. Sci. Lett. 181(1-2): 229-249.

Behar, F., Vandenbroucke, M., Tang, Y., Marquis, F., Espitalie, J., 1997. Thermal cracking of kerogen in open and closed systems: determination of kinetic parameters and stoichiometric coefficients for oil and gas generation. Org. Geochem. 26(5): 321-339.

Boreham, C.J., Edwards, D.S., Poreda, R.J., Darrah, T.H., Zhu, R., Grosjean, E., Main, P., Waltenberg, K., Henson, P.A., 2018. Helium in the Australian liquefied natural gas economy. The APPEA J. 2018, 58, 209-237.

Brown, A.A., 2010. Formation of High Helium Gases: A Guide for Explorationists, AAPG Conference, New Oleans, Louisiana, USA, pp. 11-14.

Byrne, D.J., Barry, P.H., Lawson, M., Ballentine, C.J., 2018. Determining gas expulsion vs retention during hydrocarbon generation in the Eagle Ford Shale using noble gases. Geochim. Cosmochim. Acta 241: 240-254.

Cai, Z., Clarke, R.H., Glowacki, B.A., Nuttall, W.J., Ward, N., 2010. Ongoing ascent to the helium production plateau—Insights from system dynamics. Resour. Policy 35(2): 77-89.

Cao, C., Zhang, M., Tang, Q., Yang, Y., Lv, Z., Zhang, T., Chen, C., Yang, H., Li, L., 2018. Noble gas isotopic variations and geological implication of Longmaxi shale gas in Sichuan Basin, China. Mar. Pet. Geol. 89: 38-46.

Cao, Z., Sun, X., Wang, L., Yan, C., Zhao, J., Ma, F., 2013. The gas accumulation conditions of Dongping-Niudong slope area in front of Aerjin Mountain of Qaidam Basin. Nat. Gas Geosci. 24(6): 1125-1131.

Cherniak, D.J., Pyle, J.M., 2008. Th diffusion in monazite. Chem. Geol. 256(1): 52-61.

Cherniak, D.J., Watson, E.B., 2011. Helium diffusion in rutile and titanite, and consideration of the origin and implications of diffusional anisotropy. Chem. Geol. 288(3–4): 149-161.

Craig, H., Lupton, J.E., 1976. Primordial neon, helium, and hydrogen in oceanic basalts. Earth Planet. Sci. Lett. 31(3): 369-385.

Danabalan, D., 2017. Helium: Exploration Methodology for a Strategic Resource, Durham University.

Darrah, T.H., Jackson, R.B., Vengosh, A., Warner, N.R., Whyte, C.J., Walsh, T.B., Kondash, A.J., Poreda, R.J., 2015. The evolution of Devonian hydrocarbon gases in shallow aquifers of the northern Appalachian Basin: Insights from integrating noble gas and hydrocarbon geochemistry. Geochim. Cosmochim. Acta 170: 321-355.

Darrah, T.H., Vengosh, A., Jackson, R.B., Warner, N.R., Poreda, R.J., 2014. Noble gases identify the mechanisms of fugitive gas contamination in drinking-water wells overlying the Marcellus and Barnett Shales. Proc. Natl. Acad. Sci. 111(39): 14076-14081.

Dymond, J.H., Smith, E.B., 1980. The virial coefficients of gases and mixtures. Clarendon Press, Oxford, UK.

Farley, K.A., 2000. Helium diffusion from apatite: General behavior as illustrated by Durango fluorapatite. J. Geophys. Res.: Solid Earth 105(B2): 2903-2914.

Gautheron C., Moreira M. (2002) Helium signature of the subcontinental lithospheric mantle. Earth Planet. Sci. Lett. 199, 0-47.

Gilfillan S.M.V., Ballentine C.J., Holland G., Blagburn D., Lollar B.S., Stevens S., Schoell M. and Cassidy M. (2008) The noble gas geochemistry of natural CO2 gas reservoirs from the Colorado Plateau and Rocky Mountain provinces, USA. Geochim. Cosmochim. Acta 72, 1174-1198.

Holland G., Lollar B.S., Li L., Lacrampe-Couloume G., Slater G.F. and Ballentine C.J. (2013) Deep fracture fluids isolated in the crust since the Precambrian era. Nature 497, 357-360.

Kennedy, B., Hiyagon, H., Reynolds, J., 1990. Crustal neon: a striking uniformity. Earth Planet. Sci. Lett. 98(3-4): 277-286.

Lee, J.Y., Marti, K., Severinghaus, J.P., Kawamura, K., Yoo, H.S., Lee, J.B., Kim, J.S., 2006. A redetermination of the isotopic abundances of atmospheric Ar. Geochim. Cosmochim. Acta 70(17): 4507-4512.

Li, J., Li, Z., Jia, Y., 2014. Special geological conditions and development modes of the Dongping Basement Gas Reservoirs in the Qaidam Basin. Nat. Gas Ind. 34(8): 75-81.

Li, M., Shao, L., Liu L., Lu, J., Spiro, B., Wen, H., Li Y., 2016. Lacustrine basin evolution and coal accumulation of the Middle Jurassic in the Saishiteng coalfield, northern Qaidam Basin, China. J. Palaeogeogr. 5(3): 205-220.

Lorant, F., Prinzhofer, A., Behar, F., Huc, A.-Y., 1998. Carbon isotopic and molecular constraints on the formation and the expulsion of thermogenic hydrocarbon gases. Chem. Geol. 147(3): 249-264.

Luo, X. Sun, Y., Wang, L., Xiao, A., Ma, L., Zhang, X., Wang, Z., Song, C., 2013. Dynamics of hydrocarbon accumulation in the west section of the northern margin of the Qaidam Basin, NW China. Pet. Explor. Dev. 40(2): 170-182.

Ma, F. Yan, C., Ma. D., Le, X., Huang, C., Shi, Y., Zhang, Y., Xie, M., 2015. Bedrock gas reservoirs in Dongping area of Qaidam Basin, NW China. Pet. Explor. Dev. 42(3): 293-300.

Matsuda, J.I., Nagao, K., 1986. Noble gas abundances in deep-sea sediment core from eastern equatorial Pacific. Geochem. J., 20: 71-80.

Mamyrin, B.A., Tolstikhin, L.N., 1984. Helium isotopes in nature, Elsevier ; New York pp.

Niedermann, S., Graf, T., Marti, K., 1993. Mass spectrometric identification of cosmic-ray-produced neon in terrestrial rocks with multiple neon components. Earth Planet. Sci. Lett. 118(1): 65-73.

Nuttall, W.J., Clarke, R.H., Glowacki, B.A., 2012. The Future of Helium as a Natural Resource, Taylor & Francis Group.

Ozima, M., Podosek, F.A., 2002. Noble gas geochemistry. Cambridge University Press.

Pepin, R.O., 2000. On the isotopic composition of primordial xenon in terrestrial planet atmospheres, From Dust to Terrestrial Planets. Springer, pp. 371-395.

Pinti, D.L. Beland-Otis, C., Tremblay, A., Castro, M.C., Hall, C.M., Marcil, J.S., Lavoie, J.Y., Lapointe, R., 2011. Fossil brines preserved in the St-Lawrence Lowlands, Québec, Canada as revealed by their chemistry and noble gas isotopes. Geochim. Cosmochim. Acta 75(15): 4228-4243.

Podosek, F.A., Bernatowicz, T.J., Kramer, F.E., 1981. Adsorption of xenon and krypton on shales. Geochim. Cosmochim. Acta 45(12): 2401-2415.

Reiners, P.W., Farley, K.A., Hickes, H.J., 2002. He diffusion and (U–Th)/He thermochronometry of zircon: initial results from Fish Canyon Tuff and Gold Butte. Tectonophysics, 349(1–4): 297-308.

Smith, S.P., Kennedy, B.M., 1983. The solubility of noble gases in water and in NaCl brine. Geochim. Cosmochim. Acta 47: 503-515.

Tian, J., Jian, L., Xu, Z., Guo, Z., Fei, Z., Wang, B., Wang, K., 2017. Geochemical characteristics and petroleum geologic significance of natural gas in the north margin of the Qaidam Basin. Oil Gas Geo. 38(2): 355-362.

Tian, J., Jian, L., Pan, C. Tan, Z., Zeng, X., Guo, Z., Wang, B., Zhou, F., 2018. Geochemical characteristics and factors controlling natural gas accumulation in the northern margin of the Qaidam Basin. J. Pet. Sci. Eng. 160: 219-228.

Tissot, B., Welte, D., 1984. Petroleum Formationand Occurrence (2nd. revision). Springer-Verlag, New York.

Tolstikhin, I.N., Ballentine, C.J., Polyak, B.G., Prasolov, E.M., Kikvadze, O.E., 2017. The noble gas isotope record of hydrocarbon field formation time scales. Chem. Geol. 471, 141-152.

Torgersen, T., 1980. Controls on pore-fluid concentration of ^{4}He and ^{222}Rn and the calculation of ^{4}He/^{222}Rn ages. J. Geochem. Explor. 13(1): 57-75.

Torgersen, T., Clarke, W.B., 1985. Helium accumulation in groundwater, I: An evaluation of sources and the continental flux of crustal ^{4}He in the Great Artesian Basin, Australia. Geochim. Cosmochim. Acta 49(5): 1211-1218.

Torgersen, T., Kennedy, B., 1999. Air-Xe enrichments in Elk Hills oil field gases: role of water in migration and storage. Earth Planet. Sci. Lett. 167(3-4): 239-253.

Vinogradov A. P., Ryabchikov D. I., 1962. Detection and analysis of rare elements. Oldbourne Press.

Wen, T., Castro, M.C., Nicot, J.P., Hall, C.M., Pinti, D.L., Mickler, P., Darvari, R., Larson, T., 2017. Characterizing the Noble Gas Isotopic Composition of the Barnett Shale and Strawn Group and Constraining the Source of Stray Gas in the Trinity Aquifer, North-Central Texas. Environ. Sci. Technol. 51, 6533-6541.

Yang, W., Gao, R., Guo, Q., Liu, Y., 1985. Generation, migration and accumulation of nonmarine petroleum in the Songliao Basin China. Heilongjiang science & technology press, Harbin.

Zartman, R., Wasserburg, G., Reynolds, J., 1961. Helium, argon, and carbon in some natural gases. J. Geophys. Res. 66(1): 277-306.

Zhang M., Tang Q., Cao C., Lv Z., Zhang T., Zhang D., Li Z. and Du L. (2018) Molecular and carbon isotopic variation in 3.5 years shale gas production from Longmaxi Formation in Sichuan Basin, China. Mar. Pet. Geol. 89, 27-37.

Zhang, W., Li, Y., Zhao, F., Han, W., Li, Y., Wang, Y., Holland, G., Zhou Z., 2019. Using noble gases to trace groundwater evolution and assess helium accumulation in Weihe Basin, central China. Geochim. Cosmochim. Acta 251: 229-246.

Zhou, F., Zhang, Y., Liu, Z., Sui, G., Li, G., Wang, C., Cui, S., Zhang, Y., Wang, J., Zhu, J., 2016. Geochemical characteristics and origin of natural gas in the Dongping–Niudong areas, Qaidam Basin, China. Journal of Nat. Gas Geosci. 1(6): 489-499.

Zhou, Z., Ballentine, C.J., 2006. ^{4}He dating of groundwater associated with hydrocarbon reservoirs. Chem. Geol. 226(3-4): 309-327.

Zhou, Z., Ballentine, C.J., Kipfer, R., Schoell, M., Thibodeaux, S., 2005. Noble gas tracing of groundwater/coalbed methane interaction in the San Juan Basin, USA. Geochim. Cosmochim. Acta 69(23): 5413-5428.

Zhou, Z., Ballentine, C.J., Schoell, M., Stevens, S.H., 2012. Identifying and quantifying natural CO2 sequestration processes over geological timescales: The Jackson Dome CO_2 Deposit, USA. Geochim. Cosmochim. Acta 86: 257-275.

Zwahlen, C.A., Kampman, N., Dennis, P., Zhou, Z., Holland, G., 2017. Estimating carbon dioxide residence time scales through noble gas and stable isotope diffusion profiles. Geology, 45(11): 995-998.

Figures

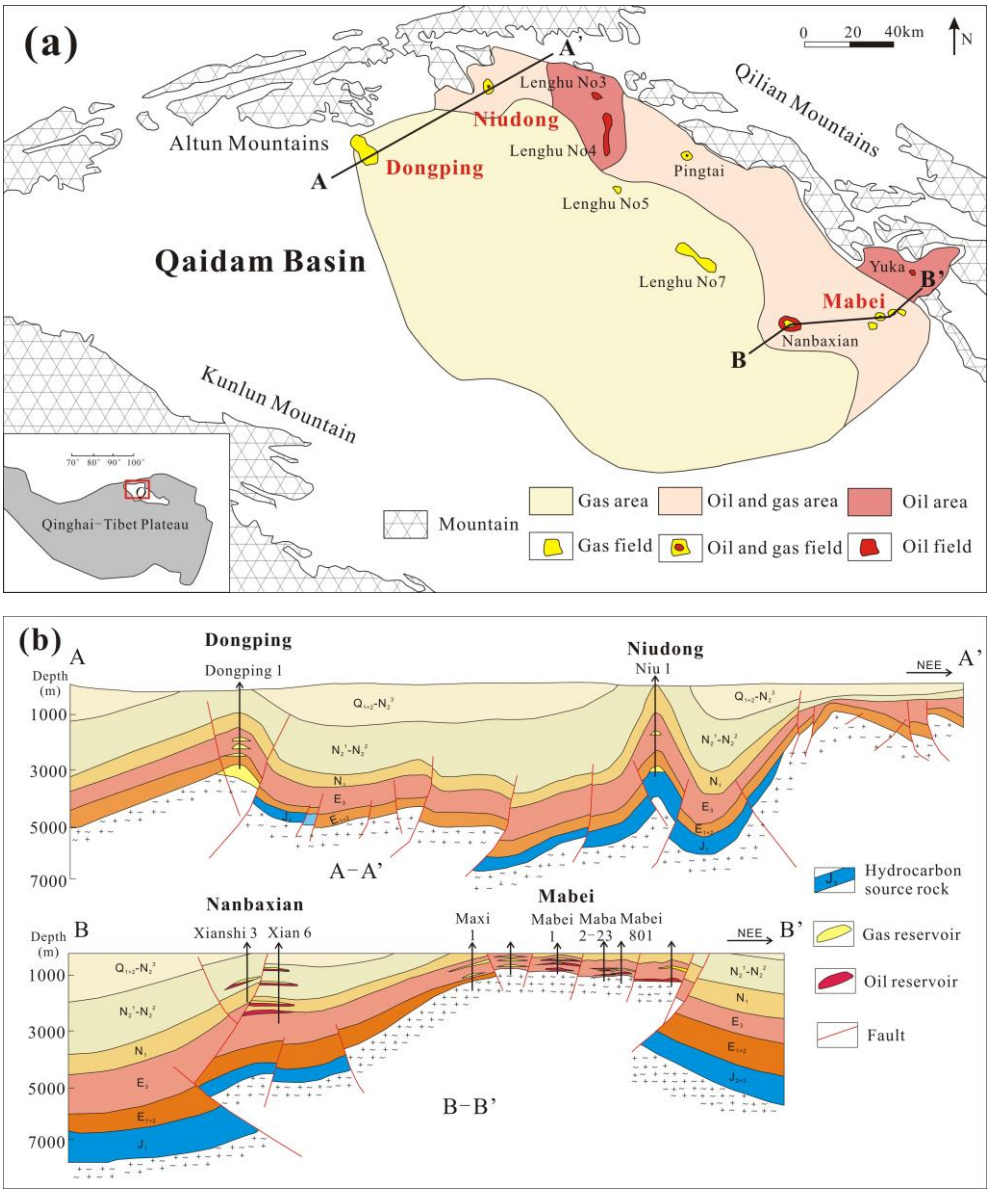

Fig. 1. (a) Geological map of the North Qaidam Basin. Gas samples were collected from the Mabei, Dongping and Niudong gas fields, which are shown in bold red font. (b) Geological cross sections of the Dongping-Niudong gas field (A-A') and the Nanbaxian-Mabei oil and gas field (B-B'). The sampled production wells in Mabei field are labelled in the B-B' cross section. Since the sample locations are close to each other in both the Dongping and Niudong gas fields, only representative wells (Dongping 1 and Niu 1) are shown in the A-A' section.

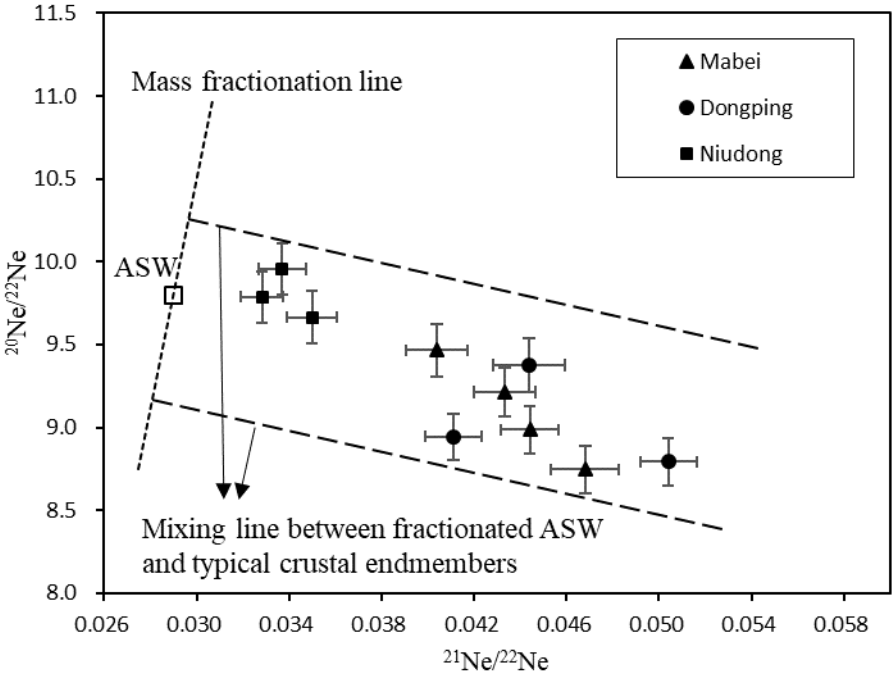

Fig. 2. Ne isotopic ratios ($^{20}Ne/^{22}Ne$ vs. $^{21}Ne/^{22}Ne$) in produced gases from the Mabei, Dongping and Niudong gas fields. The data can be explained by mixing between mass-fractionated air-saturated water (ASW) and typical crustal endmembers.

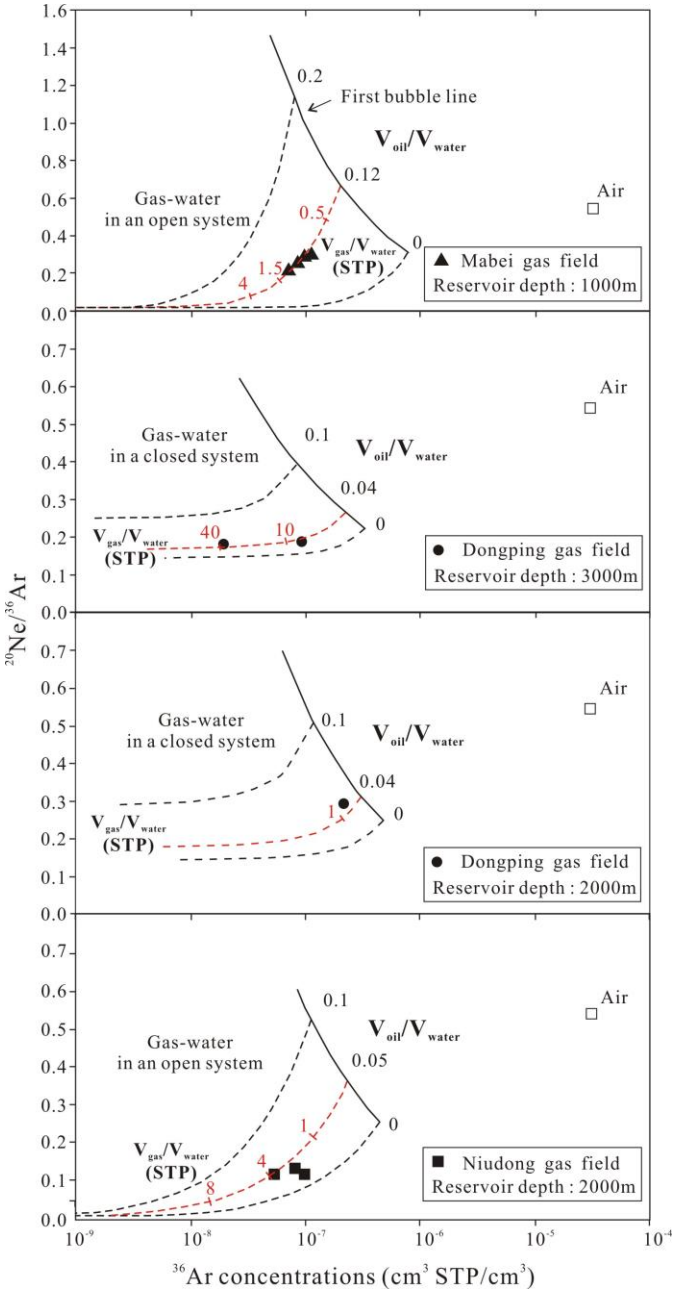

Fig. 3 Two-stage phase fractionation modelling results. Black solid line represents noble gas characteristics of the first bubble from groundwater that has equilibrated with oil before gas-water equilibrium. Dashed line indicates the noble gas features in the gas phase with different gas/water ratios, in which the red dashed line suggests the approximate model result. The V_{oil}/V_{water} ratio and V_{gas}/V_{water} ratio are labelled near the lines. Sample Dongping 3 was modelled separately in the third plot since the gas reservoir is located at a depth of ~2000m, shallower than those associated with other wells in the Dongping area (~3000m in depth).

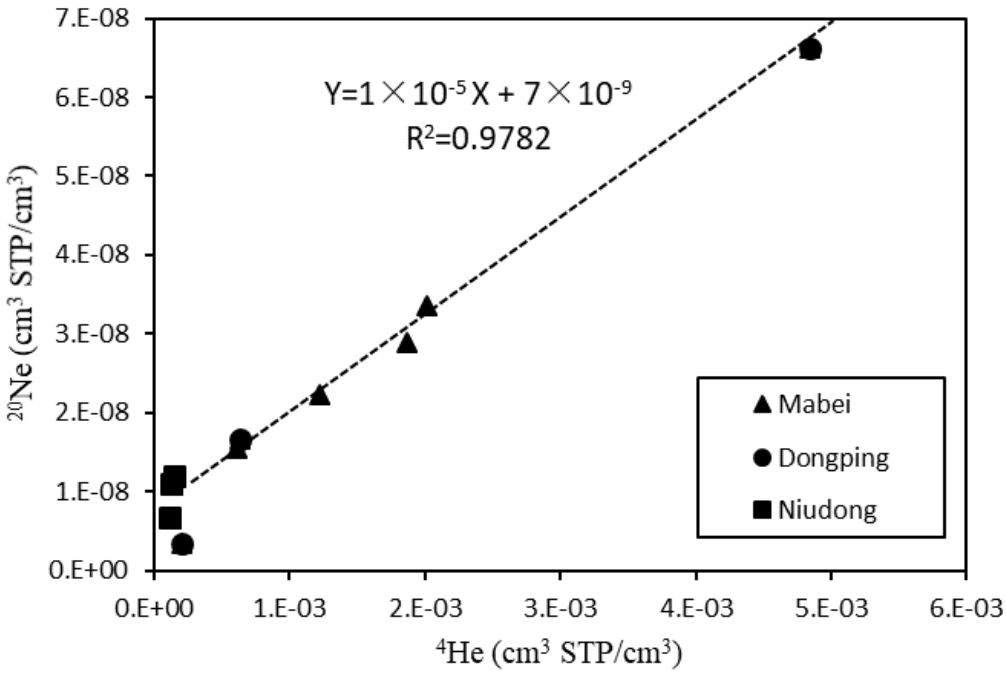

Fig. 4. The linear relationship between ^{4}He and ^{20}Ne concentrations (cm^3 STP/cm^3) in the Mabei, Dongping and Niudong gas fields.

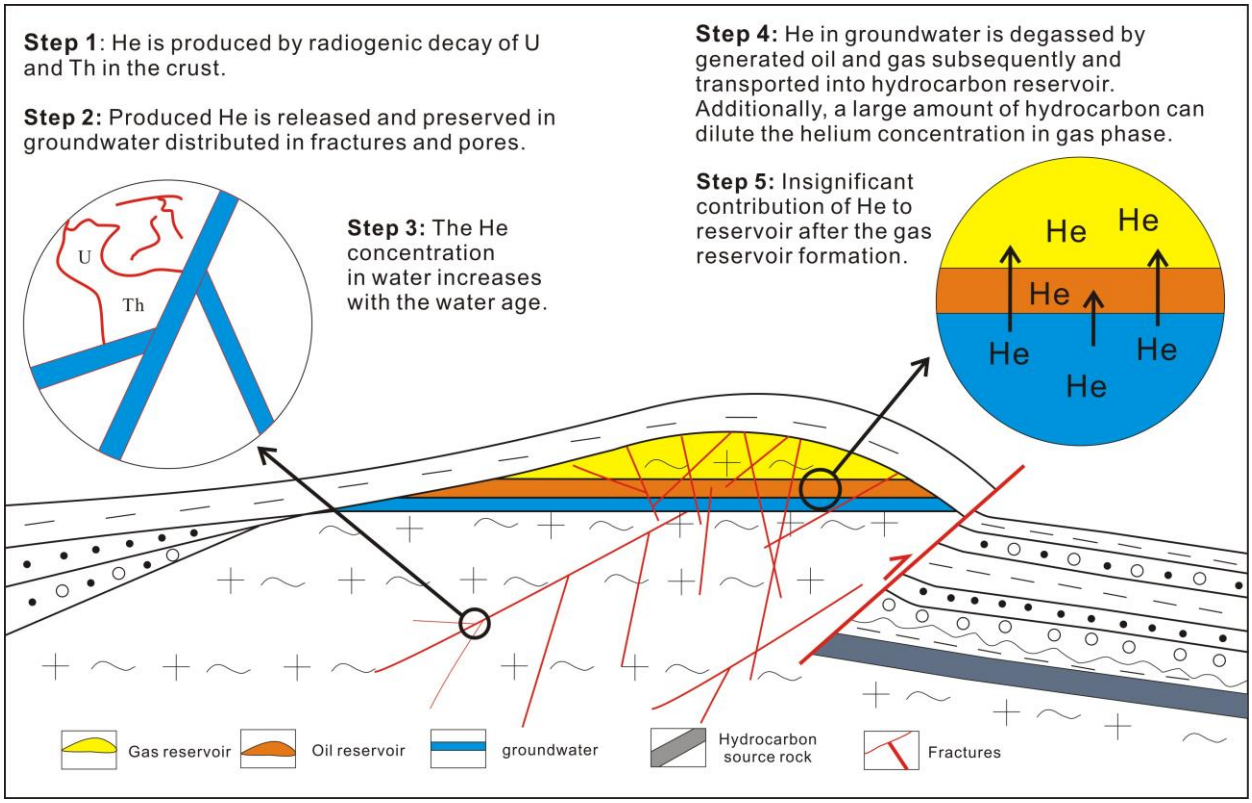

Fig. 5. Cartoon illustrating the helium accumulation processes in the North Qaidam Basin, China, which can be divided into 5 steps. See detailed discussion in Section 5.3.

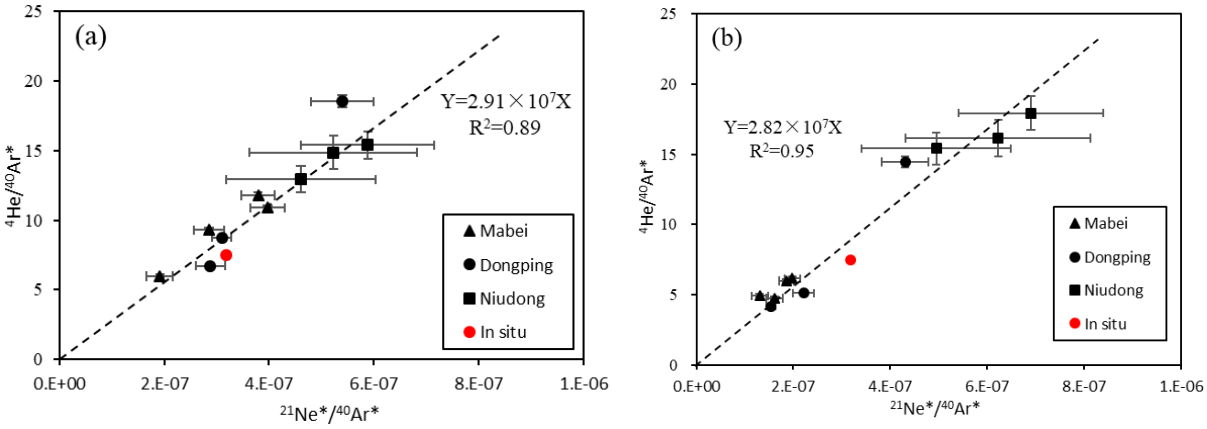

Fig. 6. (a) Measured $^{4}He/^{40}Ar^{*}$ vs. $^{21}Ne^{*}/^{40}Ar^{*}$ in the gas phase. (b) Calculated $^{4}He/^{40}Ar^{*}$ vs. $^{21}Ne^{*}/^{40}Ar^{*}$ in the initial groundwater. The red dot represents the in-situ production ratio of $^{4}He/^{40}Ar^{*}$ and $^{21}Ne^{*}/^{40}Ar^{*}$ being 7.5 and 2.81×10^{-7}, respectively. Characteristics of the measured crust-derived noble gases in gas phase as shown in plot (a) are controlled by the oil-modified groundwater-exsolution fractionation process on the base of the two kinds of sources for ^{4}He, $^{21}Ne^{*}$ and $^{40}Ar^{*}$ in groundwater and rocks shown in plot (b).

Table 1 Major gas composition data (in volume fraction, vol. %) for the three gas fields in the North Qaidam Basin.

Sample	C_1	C_2	C_3	N_2	CO_2	O_2	Gas Dryness
Mabei gas field							
Mabei 801	76.64	8.50	2.98	8.87	0.53	0.05	0.85
Maxi 1	87.63	2.76	0.39	8.54	0.30	0.03	0.96
Maba 2-23	78.83	8.59	2.93	7.41	0.10	0.02	0.85
Dongping gas field							
Dongping 171	95.18	2.48	0.39	1.15	0.10	0.05	0.97
Dongping 1	89.99	1.96	0.31	6.87	0.21	0.03	0.97
Niudong gas field							
Niu 1	89.04	6.30	1.69	1.41	0.19	0.13	0.91
Niu 1-2-10	86.97	7.60	2.12	1.54	0.25	0.16	0.89
Niu 1-2-11	86.47	7.47	2.25	2.08	0.25	0.19	0.89

Table 2 Noble gas (helium, neon, argon, krypton, and xenon) isotope systematics in gases from the North Qaidam Basin[a].

Sample	$^{4}He\times10^{-4}$	$^{20}Ne\times10^{-8}$	$^{36}Ar\times10^{-8}$	$^{84}Kr\times10^{-9}$	$^{130}Xe\times10^{-11}$	$^{3}He/^{4}He$ (R/Ra)[b]	$^{20}Ne/^{22}Ne$	$^{21}Ne/^{22}Ne$	$^{40}Ar/^{36}Ar$	$^{86}Kr/^{84}Kr$	$^{132}Xe/^{130}Xe$
	cm^3 STP/cm^3										
Air	0.05	1645	3142	650	366	1	9.80	0.029	298.56	0.305	6.61
Mabei Gas Field											
Mabei 801	18.6±0.2	2.90±0.03	9.92±0.20	3.43±0.04	4.13±0.20	0.0489±0.0010	8.75±0.14	0.0468±0.0015	2019±45	0.310±0.006	6.74±0.36
Mabei 1	12.2±0.1	2.23±0.03	8.53±0.16	3.38±0.04	5.58±0.20	0.0356±0.0014	9.21±0.15	0.0433±0.0013	1835±38	0.307±0.005	6.62±0.27
Maxi 1	6.08±0.06	1.54±0.02	7.11±0.13	3.61±0.04	5.18±0.20	0.0242±0.0010	9.47±0.16	0.0404±0.0013	1726±36	0.309±0.005	6.73±0.28
Maba 2-23	20.1±0.2	3.36±0.04	11.12±0.18	3.64±0.04	4.70±0.21	0.0372±0.0009	8.99±0.14	0.0444±0.0013	1817±35	0.301±0.006	6.84±0.33
Dongping Gas Field											
Dongping 171	2.06±0.021	0.35±0.01	1.89±0.02	0.89±0.01	2.08±0.09	0.0101±0.0003	9.38±0.16	0.0444±0.0015	883±16	0.302±0.005	6.52±0.30
Dongping 1	6.37±0.064	1.67±0.02	8.98±0.12	3.44±0.04	4.49±0.20	0.0102±0.0005	8.94±0.14	0.0411±0.0012	1350±22	0.301±0.005	6.60±0.32
Dongping 3	48.4±0.5	6.62±0.08	21.56±0.52	8.57±0.10	12.00±0.52	0.0174±0.0004	8.79±0.15	0.0504±0.0012	2862±75	0.303±0.006	6.41±0.30
Niudong Gas Field											
Niu 1	1.21±0.012	1.10±0.01	8.19±0.11	3.49±0.04	5.70±0.27	0.0148±0.0005	9.79±0.16	0.0328±0.0009	410±7	0.304±0.006	6.76±0.35
Niu 1-2-10	1.15±0.012	0.68±0.01	5.45±0.08	2.85±0.03	3.99±0.18	0.0154±0.0006	9.67±0.16	0.0350±0.0011	432±8	0.305±0.005	6.58±0.32
Niu 1-2-11	1.42±0.014	1.20±0.01	9.78±0.13	4.83±0.05	7.57±0.35	0.0146±0.0005	9.96±0.16	0.0337±0.0010	393±6	0.304±0.005	6.42±0.32

[a] 1σ errors are shown in the table after the plus/minus signs.

[b] $^{3}He/^{4}He$ ratios (R) are normalized to the air value Ra = 1.4×10^{-6}.

Table 3 Henry's constants of noble gases in water and light oil (API=34) at modeling conditions[a].

Depth (m)	Temperature (°C)	Solvent		Henry's constants				
				Helium	Neon	Argon	Krypton	Xenon
Recharge								
0	10	Salinity: 0 M NaCl	Water (dimensionless)	105	85	23	12	7
Reservoir (Mabei)								
		Salinity: 2.02 M NaCl	Water (dimensionless)	158	148	68	43	32
1000	44	Salinity: 2.02 M NaCl	Water (atm kg/mol)	4112	3857	1777	1129	842
		API: 34	Oil (atm kg/mol)	700	590	119	40	12
Reservoir (Dongping 1 and 171)								
		Salinity: 2.02 M NaCl	Water (dimensionless)	110	112	72	53	48
3000	112	Salinity: 2.02 M NaCl	Water (atm kg/mol)	3488	3553	2274	1671	1506
		API: 34	Oil (atm kg/mol)	392	358	139	49	27
Reservoir (Dongping 3 and Niudong)								
		Salinity: 2.02 M NaCl	Water (dimensionless)	134	130	74	51	42
2000	78	Salinity: 2.02 M NaCl	Water (atm kg/mol)	3853	3754	2144	1478	1220
		API: 34	Oil (atm kg/mol)	524	460	128	44	18

[a] Henry's constants of noble gases in water and oil are calculated from empirical equations from Ballentine et al. (2002) and corrected with fugacity coefficients and activity coefficients (Dymond and Smith, 1980, Smith and Kennedy, 1983).

Table 4 Volume ratios of oil to groundwater and gas to groundwater, and He concentrations in the initial groundwater.

Sample	$^{20}Ne/^{36}Ar$	f_1	f_2	V_{oil}/V_{water}	V_{gas}/V_{water} STP	V_{gas}/V_{oil}	Initial concentration in groundwater [a] (cm^3 STP/g)		
							^{4}He ($\times10^{-3}$)	$^{21}Ne^*$ ($\times10^{-11}$)	$^{40}Ar^*$ ($\times10^{-4}$)
Mabei gas field									
Mabei 801	0.286±0.006	0.24	0.47	0.12	1.21	10.06	13.9±0.1	44.7±3.6	22.6±0.6
Mabei 1	0.252±0.005	0.27	0.45	0.11	1.28	11.71	9.52±0.10	32.5±3.2	20.1±0.5
Maxi 1	0.210±0.005	0.22	0.35	0.13	1.69	13.36	9.18±0.09	24.4±3.2	18.7±0.5
Maba 2-23	0.291±0.006	0.27	0.51	0.11	1.09	9.93	11.9±0.1	37.0±3.1	19.9±0.4
Dongping gas field									
Dongping171	0.179±0.003	0.62	-	0.04	39.15	1081.28	11.1±0.1	33.1±3.6	7.69±0.2
Dongping1	0.185±0.003	0.74	-	0.02	6.81	292.97	7.05±0.07	30.6±2.9	13.8±0.3
Dongping3	0.287±0.008	0.58	-	0.04	0.71	17.20	14.0±0.2	51.8±3.0	33.6±0.9
Niudong gas field									
Niu 1	0.133±0.002	0.55	0.29	0.04	3.49	77.71	2.30±0.02	7.39±2.2	1.49±0.1
Niu 1-2-10	0.122±0.002	0.49	0.24	0.05	4.02	75.97	3.21±0.03	12.3±2.5	1.77±0.1
Niu 1-2-11	0.120±0.002	0.75	0.31	0.02	3.28	151.48	2.07±0.02	7.97±2.4	2.27±0.1

a $^{21}Ne^*$ and $^{40}Ar^*$ represent the crust-derived components of ^{21}Ne and ^{40}Ar calculated by $^{21}*Ne = {}^{21}Ne - 0.00298 \times {}^{20}Ne$ and $^{40}Ar^* = {}^{40}Ar - 298.56 \times {}^{36}Ar$.